Microsc. Microanal. 14, 27–35, 2008
DOI: 10.1017/S1431927608080173

Microscopy AND Microanalysis

A Practical Solution for Eliminating Artificial Image Contrast in Aberration-Corrected TEM

Jun Yamasaki,[1,*] Tomoyuki Kawai,[2] Yushi Kondo,[2] and Nobuo Tanaka[1]

[1]*EcoTopia Science Institute, Nagoya University, Nagoya 464-8603, Japan*
[2]*Department of Crystalline Materials Science, Nagoya University, Nagoya 464-8603, Japan*

Abstract: We propose a simple and practical solution to remove artificial contrast inhibiting direct interpretation of atomic arrangements in aberration-corrected TEM. The method is based on a combination of "image subtraction" for elimination of nonlinear components in images and newly improved "image deconvolution" for proper compensation of nonflat phase contrast transfer function. The efficiency of the method is shown by experimental and simulation data of typical materials such as gold, silicon, and magnesium oxide. The hypothetical results from further improvements of TEM instruments are also simulated. It is concluded that we can approach actual atomic structures by using the present method, that is, a proper combination of a C_s corrector, image subtraction, and image deconvolution processes.

Key words: aberration-corrected TEM, nonlinear component, image subtraction, image deconvolution, artificial image contrast, C_s-corrected TEM

Introduction

The recent development in aberration correction of magnetic lenses has caused a great improvement in point-to-point resolution of high-resolution transmission electron microscopy (HRTEM) up to the information limit, and various applications have enabled progress of structure analysis at an atomic level (Tanaka et al., 2003*a*, 2003*b*, 2004; Yamasaki et al., 2004; Hirahara et al., 2006). The current main factors limiting the resolution are specifications of the instrument such as energy spread of electron source, instability of high voltage, and mechanical vibrations, which have been improved gradually. The objective of ultimate high resolution in TEM is not only to determine accurate positions of atomic nuclei as an array of delta functions the same as in annular dark field scanning TEM (ADF-STEM), but also to reproduce potential distribution as a continuous function that has maxima corresponding to atom positions in materials. Unfortunately, artificial contrast maxima always appear at positions where no atom exists in current HRTEM images. The artificial contrast is coming from two problems based on imaging theory of phase contrast and cannot be solved even by aberration correction established presently. It is considered that improvement of resolution without solving the problems is somehow difficult and may cause misleading results in atomic-level analyses of unknown structures.

Received July 17, 2007; Accepted August 7, 2007.
*Corresponding author. E-mail: p47304a@nucc.cc.nagoya-u.ac.jp

The first of the two problems is the existence of nonlinear image components in HRTEM images. They are formed by interference between diffracted beams and do not correspond to actual atomic arrangements, as well known as half-spacing lattice fringes of gold (Spence, 1981). Solving this problem is very important in the coming era in which materials analyses will be extensively performed by aberration-corrected TEM, because the nonlinear components are highly visible in aberration-corrected TEM, as mentioned later. For eliminating the nonlinear components, some methods such as using a beam stopper or objective apertures of unique shapes were proposed previously, which are poor in versatility (Saxton, 1980; Hohenstein, 1991; Akashi et al., 2005). We proposed recently a simple and practical method in which the nonlinear components can be eliminated by a subtractive operation of two defocused images in an aberration-corrected TEM (Yamasaki et al., 2005).

The second problem is the imperfectness of a kind of phase plate formed by the defocused objective lens (Scherzer method). Apart from the above nonlinear components, phase contrast transfer function (PCTF) must be ideally flat over all two-dimensional spatial frequencies $\boldsymbol{u}$ in order to reproduce exit wavefields perfectly on the image plane. However, the actual lens PCTF is partly flat only in limited frequency regions as shown in Figure 1, and resultant images are composed of improper Fourier coefficients. Therefore, the images contain artificial contrast that does not correspond to actual atom positions. To solve the problem, a compensation technique by image processing called "im-

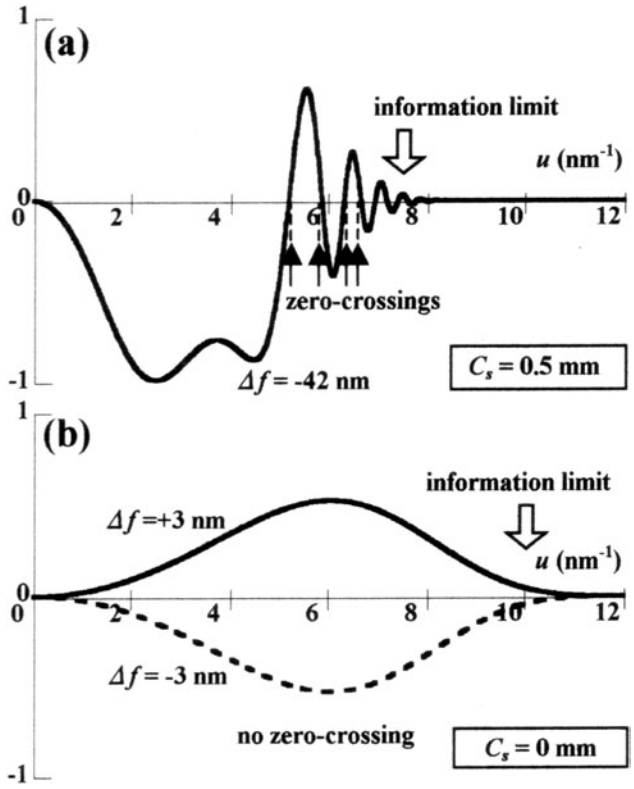

Figure 1. PCTF in (**a**) a conventional TEM (C_s = 0.5 mm, Δf = −42 nm [Scherzer defocus]) and (**b**) a spherical aberration-corrected TEM (C_s = 0, Δf = ±3 nm). (E = 200 kV, Δ = 3 nm, α = 0.5 mrad.)

age deconvolution" has been tried since the 1980s (Han et al., 1986). The method is based on an idea that a flat PCTF can be recovered by a deconvolution operation of a HRTEM image by inverse Fourier transform of the actual PCTF. Analyses of unknown structures by this method, however, have been rather difficult owing to some points such as many zero crossings in the PCTF, as mentioned in detail later.

The two problems, nonlinear components and nonflat PCTF, lead to the conclusion that structure analyses at an atomic level from only one image in HRTEM may be impossible. Some methods using through-focus images have been proposed, which, however, require the task of taking many images and numerical calculations for fitting or optimization (Coene et al., 1996; Kawasaki et al., 2001; Meyer et al., 2002; Allen et al., 2004). In this article, we propose a simple and elegant method to solve these problems by using only two defocused images in an aberration-corrected TEM.

Materials and Methods

In this study, a crystalline gold thin film and crushed silicon flakes mounted on carbon microgrids are examined by an aberration-corrected TEM, which is a thermal-field emission 200-kV TEM (JEM-2100F) equipped with an aberration corrector (CEOS GmbH) (Haider et al., 1998). The information limit of the instrument is measured by amorphous thin films to be 0.10–0.11 nm, which corresponds to about 3 nm of defocus spread (Δ). All HRTEM images in this study are recorded with a spherical aberration coefficient (C_s) of 0 ± 1.5 μm by a 1k × 1k CCD camera (Tietz Co.). Image simulations are performed by a commercial software including the second-order effects (MacTempas). Subtractive operations between defocused images are performed by Gatan Digital Micrograph. Image deconvolution operations are processed by a self-produced program.

Results and Discussion

Artificial Image Contrast by Nonlinear Components and a Novel Solution by the Subtraction Method

Interference between the direct beam and one of the diffracted beams makes a lattice fringe reflecting an actual interatomic distance in HRTEM, which is known as a linear component. Interference between two diffracted beams makes another type of a fringe differing from actual structures, known as a nonlinear component. An HRTEM image is a superposition of both types. Figure 2 is a schematic illustration for linear/nonlinear components in the simplest case in which only direct $\boldsymbol{O}$ and diffracted $\boldsymbol{g}$ and $-\boldsymbol{g}$ beams contribute to the image. If C_s = 0 and the lens is defocused by only a few nanometers, linear components made by interferences of $\boldsymbol{O}$ and $\boldsymbol{g}$, $\boldsymbol{O}$ and $-\boldsymbol{g}$ make fringes with an interval of $d = 1/g$, as shown by black curves in Figure 2b,c. When the sign of the defocus changes in an aberration-corrected TEM, PCTF is inverted perfectly, as shown in Figure 1b. This means that the intensity curves for the linear components are inverted exactly (Fig. 2b,c) and maxima correspond to positions of atoms at overfocus and minima at underfocus, respectively. The linear components disappear at exact focus because PCTF is perfectly zero over all frequencies (Fig. 2a). On the other hand, since $\boldsymbol{g}$ and $-\boldsymbol{g}$ beams always receive equal values of phase shifts from the lens, the nonlinear component made by them forms an artificial lattice fringe with an interval of $d/2 = 1/\{g - (-g)\}$ and with the same amplitude at any defocus value (gray curves in Fig. 2a–c). So a subtractive operation between two aberration-corrected images taken at $\pm\Delta f$ can eliminate the nonlinear components and leave linear components fully, as shown in Figure 2d (Yamasaki et al., 2005).

The artificial lattice fringe with an interval of $d/2$ has been known for a long time, as half-spacing fringes, for example, in gold (Spence, 1981). Validity of the "image subtraction" method proposed above has been examined by image simulations (Fig. 3a,b). The direction of electron

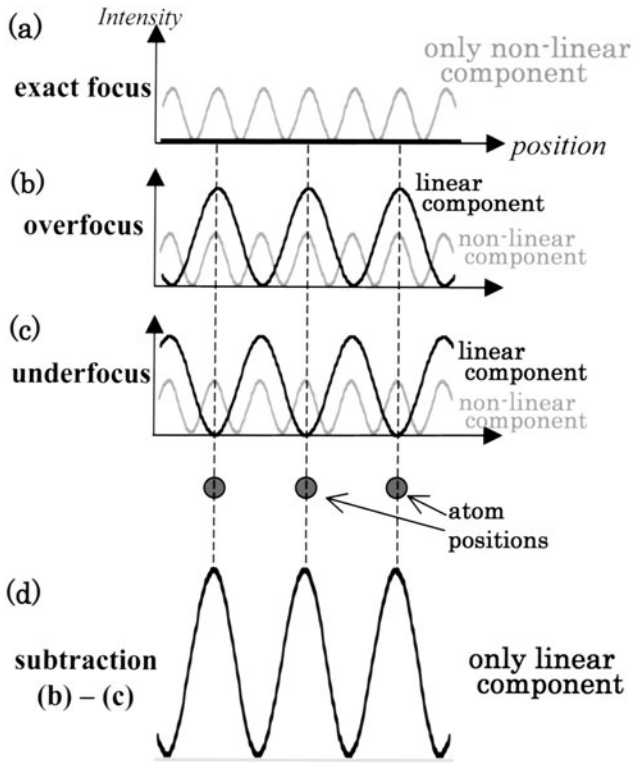

Figure 2. Schematic illustration for elimination of nonlinear components by subtractive operation between aberration-corrected over- and underfocused images.

incidence in the calculations is fixed to [051] of gold in such a way that a three-wave condition is formed in order to reduce the influence of other reflections. Figure 3a shows the simulated images formed by $\boldsymbol{O}$, $\boldsymbol{g}_{200}$, and $\boldsymbol{g}_{-200}$, and Figure 3b shows their intensity profiles perpendicular to the lattice fringes. Gold atoms exist at (200) planes with an interval of 0.204 nm, as shown by gray circles in Figure 3a and by dotted lines in Figure 3b. In all images at the exact focus and defocus of ± 3 nm, maxima of intensity appear at both atom positions and halfway positions. Intensity maxima appear only at atom positions after the subtractive operation between the underfocus and the overfocus images.

The result of the above image simulations has been confirmed also by experimental data. Figure 3c shows aberration-corrected images of gold along a [051] direction. They have been formed by using an objective aperture including only $\boldsymbol{O}$, $\boldsymbol{g}_{200}$, and $\boldsymbol{g}_{-200}$ spots. Half-spacing lattice fringes appear at areas several nanometers in thickness, though they are not so visible at thinner areas near the edge where products among amplitude of diffracted beams are small. Figure 3d shows intensity line profiles at the area indicated by white rectangles in Figure 3c. They show that the subtractive operation succeeds in eliminating the nonlinear components, though some fluctuations in peak height may be induced by amorphous material attached on the specimen surfaces.

The successful results in Figure 3 are based on the fact that interference between $\boldsymbol{g}$ and $-\boldsymbol{g}$ beams is not influenced

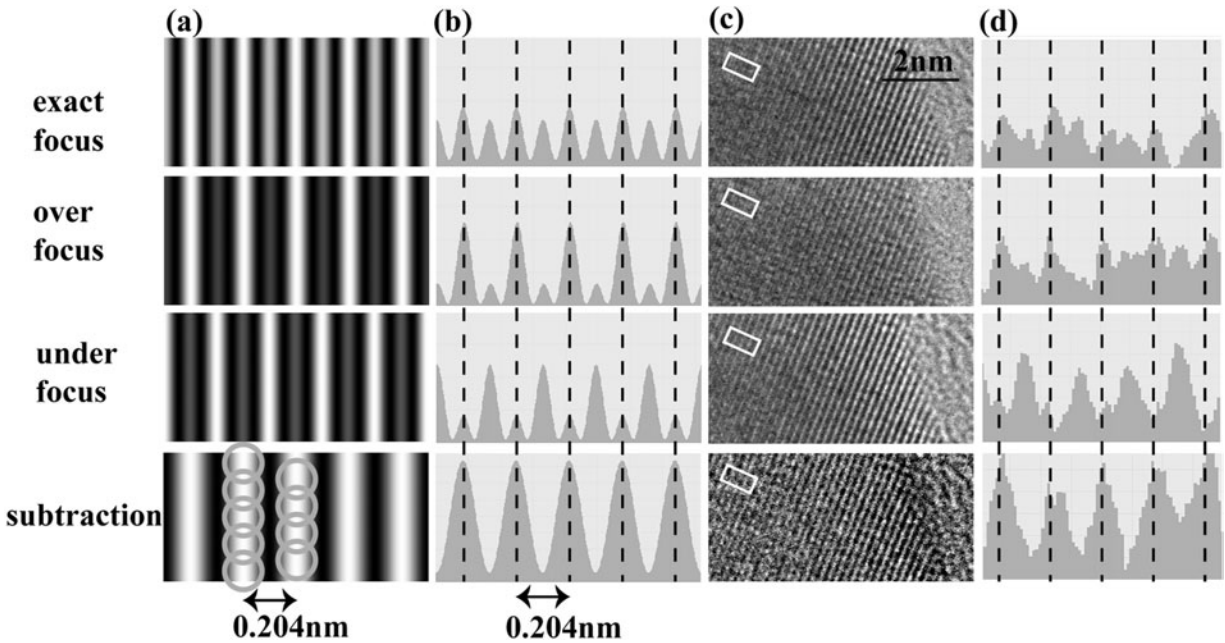

Figure 3. Elimination process of nonlinear components examined by using images of gold viewed along the [0 5 1] projection. **a:** Image simulations ($C_s = 0$, $\Delta f = \pm 6$ nm, $E = 200$ kV, $\Delta = 3$ nm, $\alpha = 0.5$ mrad). The atom positions are indicated by gray circles. **b:** Intensity line profiles of **a**. The atom positions are indicated by dotted lines. **c:** Experimental aberration-corrected images. **d:** Intensity line profiles at the area indicated by white rectangles in **c**. The atom positions are indicated by dotted lines.

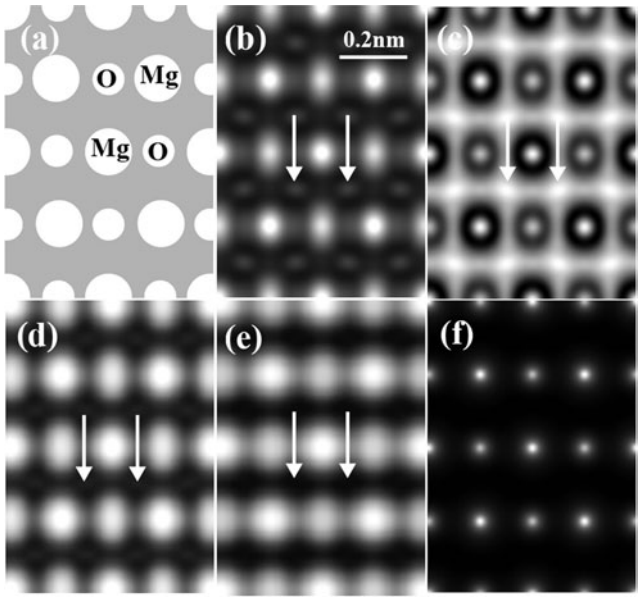

Figure 4. Application of the present method to simulated two-dimensional lattice images of MgO viewed along the [110] projection ($C_s = 0$, $\Delta f = \pm 3$ nm, $E = 200$ kV, $\Delta = 3$ nm, $\alpha = 0.5$ mrad, thickness $t = 3$ nm). (**a**) Schematic diagram of atomic arrangements; (**b**) 3-nm overfocused image; (**c**) 3-nm underfocused image; (**d**) subtraction image; (**e**) subtraction and deconvolution image; (**f**) projected potential map.

by defocus values. In the case of electron incident along a zone axis, it can be proved that interference between any $\boldsymbol{g}$ and $\boldsymbol{h}$ (not parallel to $\boldsymbol{g}$) is influenced by absolute defocus values. Therefore, two-dimensional nonlinear components can also be eliminated successfully by the present subtraction method (Yamasaki et al., 2005). This is shown in Figure 4 by using image simulations of a MgO crystal along a ⟨110⟩ direction. In over- and underfocused images in Fig. 4b,c, bright contrast clearly appears also at positions where no atom exists, as shown by white arrows. This artificial contrast becomes crucial for analysis of unknown structures. These artificial extra bright spots are reduced drastically in the subtraction image (Fig. 4d), which consists of only linear components and reproduces the actual atom positions shown in Figure 4a.

One of the characteristics of the aberration-corrected TEM is that the PCTF is free from oscillation near exact focus. It brings not only enhancement of the point-to-point resolution but also suppression of linear components due to the small values of PCTF over the whole frequency region. On the other hand, the nonlinear components remain even at exact focus (Figs. 2a and 3) and are highly visible at small defocus values. It is clear that an elimination process of nonlinear components is absolutely necessary for precise structure analysis at an atomic level. The present subtraction method is extremely useful for purifying linear components, although dynamical diffraction effects inhibit perfect elimination of nonlinear components (Yamasaki et al., 2005).

Artificial Image Contrast Caused by Oscillation of the PCTF and a Novel Solution by an Improved Deconvolution Method Combined with the Subtraction Method

As mentioned in the Introduction, the image deconvolution method has been tried for a long time in order to solve the limitation of point-to-point resolution and artificial contrast induced by PCTF oscillation. A brief overview of the method is as follows. When the weak-phase-object approximation does hold in HRTEM images, the relationship between image intensity $I(\boldsymbol{r})$ and projected potential $V_p(\boldsymbol{r})$ of a sample is written as

$$I(\boldsymbol{r}) = 1 + \frac{\pi}{\lambda E} V_p(\boldsymbol{r}) \otimes \Im^{-1}[PCTF(\boldsymbol{u})], \qquad (1)$$

where λ is the wavelength and E, the accelerating voltage of electrons. $\otimes$ and $\Im^{-1}$ denote convolution operation and inverse Fourier transform, respectively. The vector $\boldsymbol{r}$ is two-dimensional. Fourier transform of equation (1) shows

$$\Im[I(\boldsymbol{r})] = \delta(\boldsymbol{u}) + \frac{\pi}{\lambda E} \Im[V_p(\boldsymbol{r})] \times PCTF(\boldsymbol{u}). \qquad (2)$$

Equation (2) shows that, except for $\boldsymbol{u} = 0$, Fourier transform of $V_p(\boldsymbol{r})$ can be obtained by dividing Fourier transform of $I(\boldsymbol{r})$ by PCTF($\boldsymbol{u}$), which is the product of $\sin \chi(\boldsymbol{u})$ (wave abberation) and an envelope functions due to chromatic aberration and beam convergence in the weak-phase-object approximation. However, this method has the following three problems.

The first one comes from many zero crossings in the oscillating PCTF. Figure 1a shows a typical PCTF in a conventional TEM ($E = 200$ kV, $C_s = 0.5$ mm, $\Delta f = -42$ nm [Scherzer defocus], defocus spread $\Delta = 3$ nm, convergence semiangle $\alpha = 0.5$ mrad). It includes many zero crossings, as shown by arrows, which induce divergence in the division process. As one of the solutions, images in which none of the zero crossings are located in the vicinity of any main Fourier spots of crystalline samples should be selected carefully from a through-focus series (Tang et al., 2006). This method cannot, however, be applied to analyzing unknown structures, because it is unknown where the Fourier spots appear. The aberration-corrected TEM solves the problem, because there is no PCTF oscillation up to the information limit. Figure 1b shows that the PCTF in an instrument with $\Delta = 3$ nm has no zero crossing if absolute values of defocus are less than several nanometers. An aberration-corrected TEM makes it possible to carry out the image deconvolution process properly over all frequency regions. This is a great advantage of the aberration-corrected TEM in the image deconvolution method.

The second problem for the image deconvolution process is nonlinear components, as discussed above. A deconvolution process without elimination of nonlinear

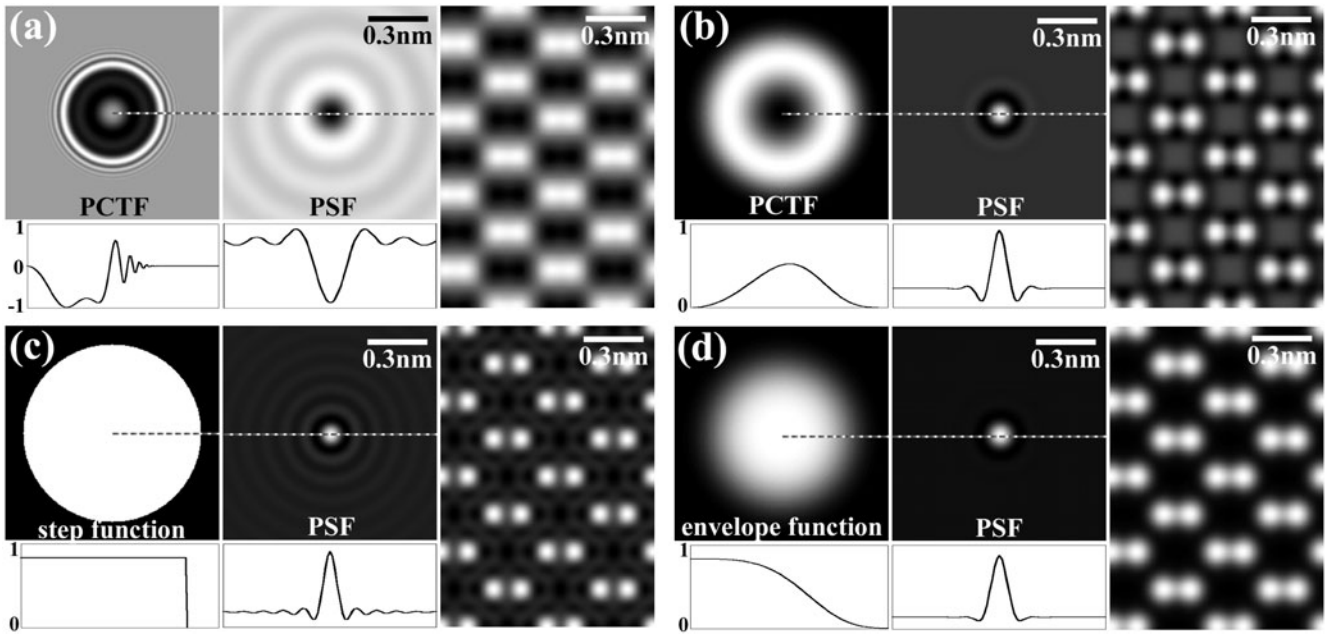

Figure 5. Filtering functions, PSFs, and simulated images of silicon from [110] ($t = 2$ nm) (**a**) in a conventional TEM ($C_s = 0.5$ mm, $\Delta f = -42$ nm); (**b**) in an aberration-corrected TEM ($C_s = 0$, $\Delta f = \pm 3$ nm) combined with the subtractive operation; (**c**) after a conventional deconvolution method; and (**d**) after the present improved deconvolution method. Profiles along the dotted lines in each image are also shown.

components induces an improper increase of the nonlinear components and the resultant artificial images. Fortunately, this problem can be solved by our subtraction process described above. Because PCTFs in two images used in the subtraction process are perfectly inverted with respect to each other in the aberration-corrected TEM, the PCTF used in the deconvolution process has the same shape.

The third problem is artificial contrast induced by so-called Fourier termination effects in the deconvolution process. Use of point spread functions (PSFs) is helpful for understanding the issue. The two-dimensional expression of the PCTF in Figure 1a ($E = 200$ kV, $C_s = 0.5$ mm, $\Delta f = -42$ nm [Scherzer defocus], $\Delta = 3$ nm, $\alpha = 0.5$ mrad) is shown in Figure 5a. The two-dimensional PCTF is a kind of filtering function, and the inverse Fourier transform of the PCTF is the PSF, which should be convoluted onto the projected potential $V_p(\boldsymbol{r})$, as shown in equations (1) and (2) as the linear approximation. The shape of the PSF is not monotonically decreasing, but includes oscillations, which should cause artificial maxima in the image formed by linear components. Moreover, nonlinear components are overlapped in the image. It may be rather difficult to eliminate these complicated artifacts and to recover proper structure images by any kind of processings of single HRTEM images. On the other hand, a C_s corrector is an effective hardware to get image contrast more similar to real atom structures due to suppression of both PCTF oscillation and nonlinear components, if combined with the present image subtraction. As shown in Figure 5b, however, there is still some uncertainty in correspondence between atomic positions and contrast maxima due to the remaining oscillation in the PSF. In a conventional deconvolution process, a Fourier transform of an image is divided by the product of $\sin \chi(\boldsymbol{u})$ and the envelope function. This procedure results in flat filtering function up to the information limit, which is a kind of step function due to lack of information beyond the information limit (Fig. 5c). In this case, artificial image contrast is induced by oscillations in the PSF, expressed by a kind of "sinc" function as the Fourier transform of the step function. This is the Fourier termination problem in the conventional deconvolution method.

In the present study, we propose the deconvolution process in which a Fourier transform of an image is divided by $\sin \chi(\boldsymbol{u})$ itself in place of a product of $\sin \chi(\boldsymbol{u})$ and the envelope function. This procedure makes an improved filtering function with the shape of the envelope function. The PSF by the envelope function has a rather ideally damping nature shown in Figure 5d. Contrast maxima appear only at actual atomic positions in the example image. This new deconvolution procedure has another advantage in that we do not need to measure the actual envelope function of the instrument. Full width at half maximum (FWHM) of the main peaks in PSF in Figure 5d is slightly larger than those in Figure 5b,c. This slight degradation of image resolution is an unavoidable issue for elimination of all kinds of artificial contrast maxima. In the viewpoint of exclusion of those kinds of artifacts in principle, Gaussian function may be ideal as a filtering function, because Fourier transform of a

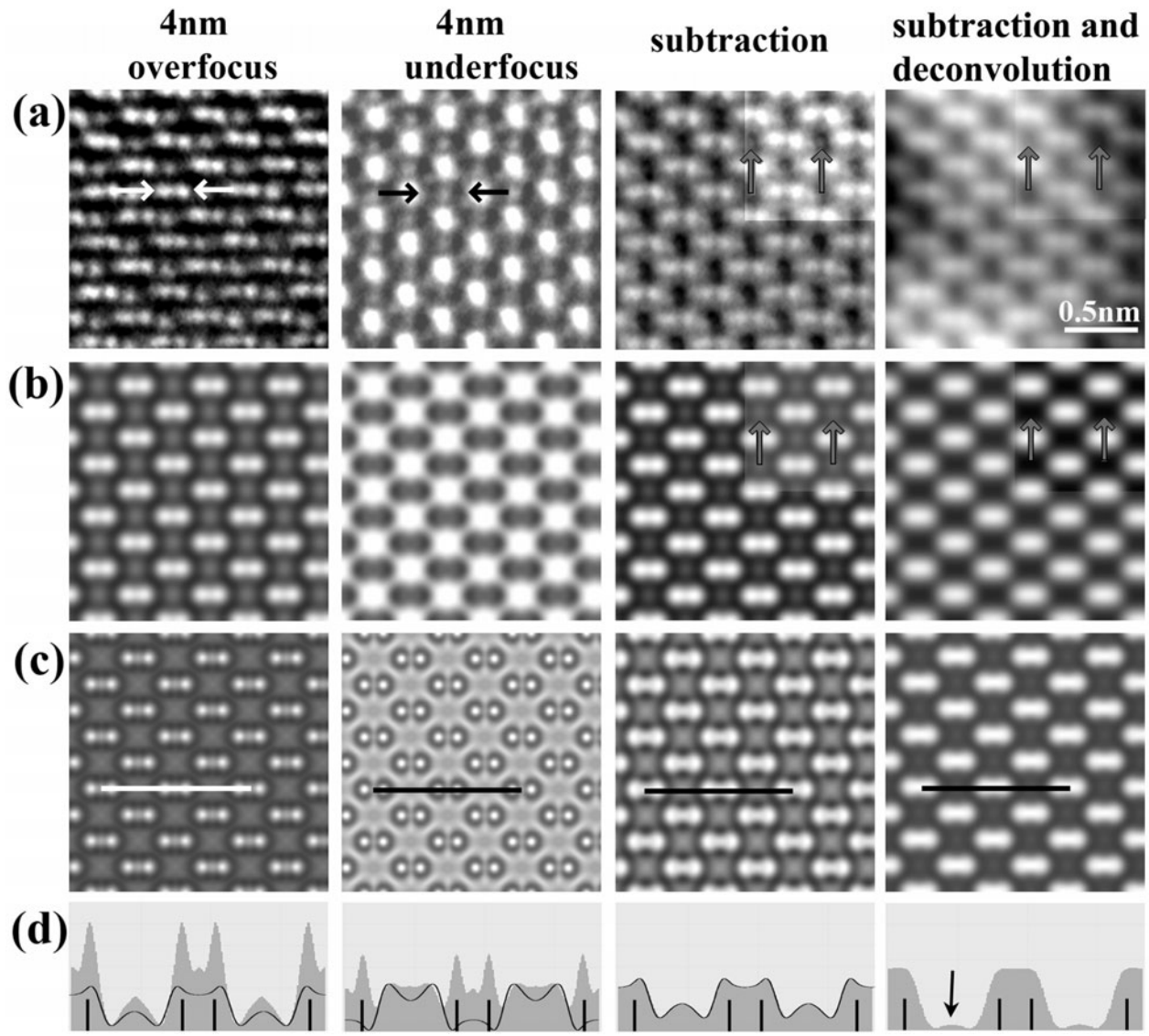

Figure 6. Subtraction and deconvolution processes for images of silicon viewed along the [110] projection. **a:** Experimental aberration-corrected TEM images. **b:** Simulated images with mechanical vibrations. **c:** Simulated images without mechanical vibrations. **d:** Intensity line profiles along the lines in **c**. In **a** and **b**, contrast is partly enhanced in the some areas around the gray arrows.

Gaussian is also a Gaussian, which has no oscillation. Use of the Gaussian function is, however, less practical than use of the envelope function because of more broadening of the PSF and the additional task to measure the information limit experimentally.

Figure 4e shows a result of the present deconvolution process applied to the subtraction image in Figure 4d. The extra bright spots (arrows) that slightly remain even after the subtractive operation are perfectly eliminated in the deconvolution image. Moreover, the elliptic contrasts at the positions of oxygen atoms are corrected to be a spherical shape by the present deconvolution process. The shape corresponds to isotropic blurring of the projected potential map of the spherical ion shape shown in Figure 4f.

Experimental Evidence of the Efficiency of the Subtraction and Deconvolution Method

The efficiency of the present method is proved experimentally by using [110] images of silicon (Fig. 6a). Black and white dumbbells of silicon are clearly shown (black and white arrows) in the aberration-corrected experimental images at 4 nm under- and overdefocus, in which other extra contrast, however, appears. The subtractive operation between them eliminates the extra contrast except for bright spots at the center of six-membered rings formed by silicon columns, as shown by the gray arrows in Figure 6a. It is considered that the bright spots come from nonflat PCTF at $\Delta f = 4$ nm. They are successfully eliminated by the following

deconvolution process. In the image after deconvolution, contrast maxima appear only at the actual atom positions. Figure 6b shows image simulations corresponding to the experimental Figure 6a. The blurring effect caused by mechanical vibration is added to the images in such a way that the images before the subtraction fit well to experimental ones. The thickness of the area shown in Figure 6a is estimated to be about 7 nm based on the fitting. Both the subtraction images and deconvolution images in simulation reproduce well the experimental ones. There is, however, a slight discrepancy between the experimental data and simulations in terms of separation distance of the silicon dumbbells in the deconvolution images. The origins of the discrepancy are suspected to be some factors not considered in the simulations, such as slight tilt from the exact zone axis.

Influence of Hypothetical Improvements in TEM Specifications

In the previous section, we proposed a novel method to overcome the problems based on HRTEM imaging theory and have shown the efficiency of the method by experiments and simulations. In this section, we simulate the results expected in the near future when the limitations from the chromatic aberration and instability of instruments should be improved (Mook & Kruit, 1999; Haider & Muller, 2005). If an instrument is stabilized enough that mechanical vibration considered in Figure 6b can be ignored, then the results shown in Figure 6c are expected. In the aberration-corrected defocused images, decrease of blurring by mechanical vibration makes fine patterns formed by nonlinear components strongly visible. The efficiency of the subtractive operation is remarkable in this situation. Figure 6d shows intensity profiles along the lines indicated in Figure 6c. The profile of linear components in the subtraction image shown as a solid curve is overlapped on that of the overfocused image. The inverted profile is also overlapped on that of the underfocused image. The atom positions are also shown by vertical bars. It indicates clearly how much our ordinary HRTEM observations depend on nonlinear components. Nonlinear components include spatial frequencies that are twice as large as linear components, because they are interference between diffracted beams such as $\boldsymbol{g}$ and $-\boldsymbol{g}$. Thus, the resolution of subtraction images is naturally degraded to a value of twice that in the original one. Moreover, because the PCTF in an aberration-corrected TEM emphasizes the periodicity of lattices more selectively than lower spatial frequencies (Fig. 1b), the deconvolution process using proper filtering functions to eliminate artificial contrast causes slight degradation of the resolution. It should be noted that the resultant lower resolution, that is, the broader PSF in Figure 5d, is inherent in the instrument. This situation indicates that we have always been making HRTEM observations with improper resolution by using artificial contrast. Extra peaks seen slightly in the deconvolution image (black arrow in Fig. 6d) are considered to be induced by dynamical diffraction effects, because such artificial peaks do not appear in simulated deconvolution images of thinner samples, as shown in Figure 5d.

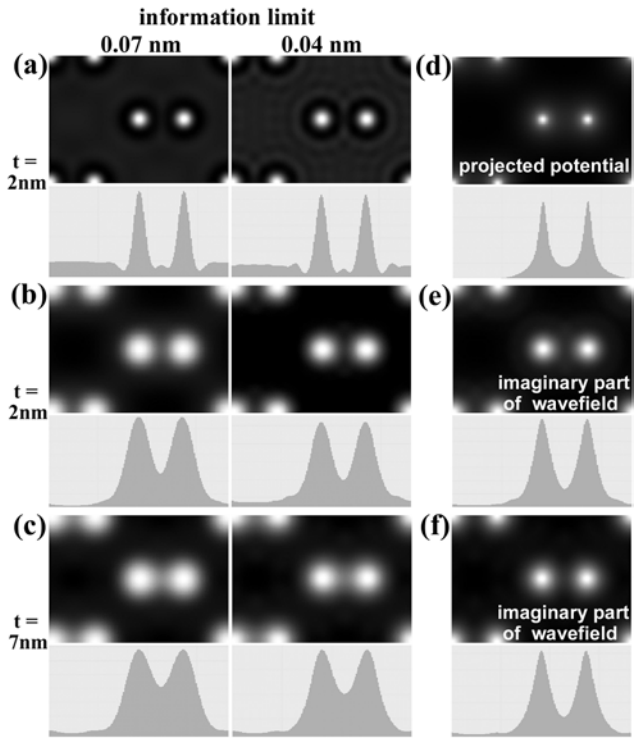

Figure 7. Influence of extension of information limit examined by simulations. Defocus values in **a–c** are 0.5 nm. The sample thickness is 2 nm in **a**, **b**, and **e** and 7 nm in **c** and **f**. **a:** Original aberration-corrected underfocus images and intensity line profiles along the horizontal center lines in the images. **b,c:** Images and line profiles after the subtraction and deconvolution process. **d:** The projected potential map and line profile. **e,f:** The imaginary parts of the exit wavefields and the line profiles.

The present information limit of our instrument is about 0.1 nm at 200 kV accelerating voltage, which corresponds to about 3 nm defocus spread. We simulate hypothetical images when further extension of the information limit is brought about by improvements of the instrument and when corrections of C_5 (fifth-order spherical aberration) and so forth are achieved (Rose, 1990). Figure 7a,b shows comparisons between simulated aberration-corrected images and the subtraction and deconvolution images at various values of the information limit. The sample thickness in the calculation is set to 2 nm in order to minimize dynamical diffraction effects. Despite extension of the information limit, the unnatural valleys of the intensity always remain around the peaks in the aberration-corrected images in Figure 7a. In contrast, the image intensity after the subtraction and deconvolution processes converges on the imaginary part of the exit wavefield in Figure 7e, which is the ultimate objective within the limit of the weak-phase-object approximation. Moreover, extension of the information limit

causes a decrease of the artificial peak shown in Figure 6d and clear separation of the dumbbells even when the sample thickness is 7 nm, as shown in Figure 7c,f. In previous researches, validity of each method, the image subtraction and the image deconvolution, has been confirmed up to several nanometers in thickness by simulation and theoretical studies (Hu & Tanaka, 1999; Yamasaki et al., 2005). It is considered that the present method is available even when the specimen thickness is a little beyond the limit of the weak-phase-object approximation, that is, several nanometers for light-element materials such as Si and MgO.

The imaginary part of the exit wavefield (Fig. 7e,f) is indeed a little blurred from the projected potential (Fig. 7d) as the result of quantum mechanical scattering. For example, FWHM of phase modulation in exit wavefields was calculated to be about 0.6 nm after transmission of 200 keV electrons through a silicon crystal of about 2 nm in thickness, though FWHM of the projected potential of a silicon atom is about 0.4 nm (Lentzen & Urban, 2006). The present method helps us to approach the resolution limit based on such physical scattering beyond the difficulties in TEM imaging even with aberration correction.

Conclusion

We have proposed a novel solution for removing artificial contrast in an aberration-corrected TEM that inhibits direct observations of atomic arrangements. The method is based on a combination of "image subtraction" for elimination of nonlinear components and newly improved "image deconvolution" for proper compensation of nonflat phase-contrast-transfer function. The efficiency of the method has been proved by experimental and simulation data of typical materials such as gold, silicon, and magnesium oxide thin films. The subtraction and deconvolution process can reproduce the images related to the actual structures with some intrinsic blurring. It is concluded that the method is applicable even when specimen thickness is beyond the limit of the weak-phase-object approximation. We can approach actual atomic structures by using the present method, that is, a proper combination of a C_s corrector, the image subtraction, and the image deconvolution.

Acknowledgments

The authors thank Dr. K. Saitoh, Dr. K. Hirahara, and Prof. T. Tanji in Nagoya University for their help. The present study is partly supported by Grant-in-Aid for Scientific Research (A) (No. 17201022) and Grant-in-Aid for Exploratory Research (No. 19656007) by the Japan Society for the Promotion of Science, and Grant-in-Aid on Priority Areas "Materials Science of Bulk Metallic Glasses" (No. 18029011) by the Ministry of Education, Culture, Sports, Science and Technology, Japan.

References

Akashi, T., Sugawara, A., Kasai, H., Yoshida, T., Matsuda, T., Togawa, Y., Harada, K. & Tonomura, A. (2005). Confirmation of information transfer using lattice images. *Appl Phys Lett* **87**, 174101.

Allen, L.J., Mcbride, W., O'leary, N.L. & Oxley, M.P. (2004). Phase retrieval from images in the presence of first-order vortices. *Ultramicroscopy* **100**, 91–104.

Coene, W.M.J., Thust, A., Op De Beek, M. & Van Dyck, D. (1996). Maximum-likelihood method for focus-variation image reconstruction in high resolution electron microscopy. *Ultramicroscopy* **64**, 109–135.

Haider, M. & Muller, H. (2005). Is there a road map of aberration correction towards ultra-high resolution in TEM and STEM? *Proceedings of the Microscopy and Microanalyis Meeting 2005*, CD 546.

Haider, M., Rose, H., Uhlemann, S., Kabius, B. & Urban, K. (1998). Toward 0.1 nm resolution with the first spherically-corrected transmission electron microscope. *J Electron Microsc* **47**, 395–405.

Han, F.S., Fan, H.F. & Li, F.H. (1986). Image-processing in high-resolution electron-microscopy using the direct method. (II) Image deconvolution. *Acta Cryst A* **42**, 353–356.

Hirahara, K., Saitoh, K., Yamasaki, J. & Tanaka, N. (2006). Direct observation of six-membered rings in the upper and lower walls of a single wall carbon nanotube by spherical aberration-corrected HRTEM. *Nano Lett* **6**, 1778–1783.

Hohenstein, M. (1991). Reconstruction of the exit surface wave function from experimental HRTEM micrographs. *Ultramicroscopy* **35**, 119–129.

Hu, J.J. & Tanaka, N. (1999). A study of the validity of the image deconvolution method on the basis of channeling theory for thicker crystals. *Ultramicroscopy* **80**, 1–5.

Kawasaki, T., Takai, Y., Ikuta, T. & Shimizu, R. (2001). Wave field restoration using three-dimensional Fourier filtering method. *Ultramicroscopy* **90**, 47–59.

Lentzen, M. & Urban, K. (2006). Contrast transfer and resolution limits for sub-Angstrom high-resolution transmission electron microscopy. *Proceedings of the Microscopy and Microanalyis Meeting* 12, CD1456.

Meyer, R.R., Kirkland, A.I. & Saxton, W.O. (2002). A new method for the determination of the wave aberration function for high resolution TEM (I). *Ultramicroscopy* **92**, 89–109.

Mook, H.W. & Kruit, P. (1999). On the monochromatisation of high brightness electron sources for electron microscopy. *Ultramicroscopy* **78**, 43.

Rose, H. (1990). Outline of a spherically corrected semiaplanatic medium-voltage transmission electron-microscope. *Optik* **85**, 19.

Saxton, W.O. (1980). Correction of artefacts in linear and nonlinear high resolution electron micrographs. *J Microsc Spectrosc Electron* **5**, 661–670.

Spence, J.C.H. (1981). *Experimental HREM*. Oxford: Clarendon Press, p. 126.

Tanaka, N., Yamasaki, J., Fuchi, S. & Takeda, Y. (2003*a*). First Observation of InGaAs quantum dots in GaP by spherical aberration-corrected HRTEM in comparison with ADF-STEM and conventional HRTEM. *Microsc Microanal* **10**, 139–145.

Tanaka, N., Yamasaki, J., Kawai, T. & Pan, H.Y. (2004). The first observation of carbon nanotubes by spherical aberration-corrected high-resolution transmission electron microscopy. *Nanotechnology* **15**, 1779–1784.

Tanaka, N., Yamasaki, J., Usuda, K. & Ikarashi, N. (2003*b*). First observation of SiO_2/Si(100) interfaces by spherical aberration-corrected high-resolution transmission electron microscopy. *J Electron Microsc* **52**, 69–73.

Tang, C.Y., Chen, J.H., Zandbergen, H.W. & Li, F.H. (2006). Image deconvolution in spherical aberration-corrected high-resolution transmission electron microscopy. *Ultramicroscopy* **106**, 539–546.

Yamasaki, J., Kawai, T. & Tanaka, N. (2004). Direct observation of a stacking fault in $Si_{1-x}Ge_x$ semiconductors by spherical aberration-corrected TEM and conventional ADF-STEM. *J Electron Microsc* **53**, 129–135.

Yamasaki, J., Kawai, T. & Tanaka, N. (2005). A simple method for minimizing non-linear image contrast in spherical aberration-corrected HRTEM. *J Electron Microsc* **54**, 209–214.